Shark-Fin Antenna for Railway Communications in LTE-R, LTE, and Lower 5G Frequency Bands

Ashwini K. Arya[1, 2], Seongjin Kim[3], Sungik Park[1, 2], Donghoon Kim[1, 2], Rehab S. Hassan[1, 2], Kyeongjun Ko[3], and Sanghoek Kim[1, 2, *]

Abstract—This paper presents a design study of a shark-fin antenna for future railway communications. Three specific bands are considered here as LTE-R (700 MHz), LTE (2100 MHz), and Lower 5G band (3500 MHz). A 3-D metallic structure using the 3D printing technique has been designed and fabricated for the consideration of the required bands. The volume size of the antenna element is $163 \times 61.9 \times 10 \, \text{mm}^3$. The multi-physical simulations in terms of the smooth air flow and lower drag coefficient are performed for analyzing the need of shark-fin radome cover. More than 70 MHz bandwidth was observed for the LTE-R band and also a wide band response from 1.4 GHz to 4.2 GHz was observed that cover the required bands well, i.e., the LTE, and Lower 5G band. The proposed shark-fin antenna results in the expected omnidirectional radiation pattern in the horizontal plane, with the radiation efficiency of 71.7%, 92.6%, and 96.4% in the railway environment for the LTE-R, LTE, and Lower 5G band frequency, respectively.

1. INTRODUCTION

The demand for high-speed wireless communication between the trains and the outside world is increasing with tremendous speed, and antenna element becomes an important part of these systems [1]. For the coverage of various bands (like, LTE-R, LTE, and Lower 5G bands, etc.), a multiband antenna or wideband antenna can be used for the communication purposes [2, 3]. LTE (long term evolution), which is used widely in the communication systems such as 4G wireless services, classifies an LTE-R band specifically dedicated to the railways as a communication network to improve the network capacity for enabling the enhanced performance [4]. Moreover, newly introduced 5G networks focus on the increasing bandwidth and higher data rates and enhanced mobile broadband services, etc. [5]. Vehicular antennas are required to work at multiple frequency bands to support various communication schemes. Also, in the recent development of electronics products and systems electrostatic discharges (ESD) are of enormous interest. These discharges can enter into the system via the antenna element. For the railway antenna that is mounted on the rooftop, DC grounding to bypass the ESD problem must be considered as a mandatory requirement [6, 7]. In this work, the Inverted F-Antenna (IFA) is chosen for our antenna structure, due to reduced size (especially low height), robust structure, multiband operations, and being DC-grounded inherently [8, 9]. Another practical aspect for the design of vehicular antenna is the antenna cover structures. The cover structure is used to minimize the perturbation of the air flow by the antenna along with the advantage of weatherproof and environment sealing [10, 11]. The aerodynamic resistance, quantified by a factor called *drag coefficient*, by the antennas cover should be minimized to save the operational energy and to avoid potential damages of antennas. The design

of a good vehicular antenna, requiring the high electrical performance of multi-band operations [12–16], as well as the multi-physical simulation is technically challenging.

In this work, a shark-fin antenna has been designed for covering three bands; LTE-R, LTE, and Lower 5G band. The simulation study has been carried out with the Autodesk Flow Design [17] for mechanical air flow simulation, and CST Microwave Studio [18] and Ansys HFSS [19] for electromagnetic simulations. The design procedure of the antenna is explained in great detail. As expected from the antennas to have an omnidirectional behavior in the horizontal plane for railway application [20], the radiation pattern was measured to be almost omnidirectional in an anechoic chamber. The position of the antenna installation is considered on the rooftop of trains [21–23]. To ensure the functionality of the antenna in the presence of a large metal surface of train, the frequency response was tested outdoor on the roof of real train. The proposed single feed multiband antenna could offer the plug and play device as of the rooftop mounted antennas for communication to off-track mounted antennas for the future railway communications.

The paper is organized as follows. The shark-fin cover design for the antenna is studied in Section 2. Antenna design study with the shark-fin cover and geometrical parameters are discussed in Section 3. Section 4 describes the measurement results and discussion for the proposed shark-fin antenna along with the train-roof installation scenario. Lastly, the conclusion is presented in Section 5.

2. SHARK-FIN COVER DESIGN

The purpose of the shark-fin shaped cover is to have the lower air resistance on the antenna element. By the definition in the literature, the air resistance describes the forces that are in opposition to the relative motion of an object as it passes through the air. Air resistance, or drag, is dependent on a number of factors including the density of the air, the area of the object, its velocity, and other properties of the object. It is important to have a less drag coefficient for the lower air resistance [10]. The drag coefficient is a dimensionless quantity that represents the amount of drag or resistance of an object in a fluid environment, such as air or water. The drag coefficient C_d is associated with a particular surface area and is defined as

$$C_d = F\frac{2}{\rho A v^2},\tag{1}$$

where F is the drag force, i.e., the force component in the direction of fluid flow velocity; ρ is the density; v is the velocity; and A is the frontal area. The lower drag coefficient indicates that the object will have less aerodynamic drag, which implies the requirement of less energy to impel the object. Higher values indicate a larger resistance to the flow, which in turn means that more energy is required to push the object at the required speed.

In this work, two covers (rectangular box and shark-fin) are designed and compared for covering the antenna element. Both covers are made in such a way that they should cover the complete antenna element and fixed well on the finite ground plane (total required size of $250 \times 95 \times 90\,\text{mm}^3$). The acrylonitrile butadiene styrene (ABS) material with dielectric permittivity of 2.1 is used for the analysis of covers. The ABS plastic material is low cost, easy to machine, and has ideal material for structural applications [24]. Rectangular box cover with the air incident area of $87(\text{height}) \times 64(\text{width})\,\text{mm}^2$ and shark-fin shaped covers (the side view can be seen in Figs. 1(a)–(b) for both type of covers) are made of the same material.

The air flow mechanism study is carried out by the Autodesk Flow Design software for various values of the wind speed in the direction as represented by black arrows in Fig. 1. In this figure, the study for wind speed of $50\,\text{m/s}$ is shown for reference. The color bar shows the velocity of air (colored lines show the air particles movement). In the case of the shark-fin cover, it can be observed that the air flow is smooth (uniform flow of air through the surface) as compared to the rectangular box cover. In the rectangular box cover, the air flow is not uniform (more intensity can be seen at the back side of the object-right side) and would result in the larger drag force on the object and thereby increase the air resistance. The respective drag coefficient to study the air resistance is observed for the same and plotted in Fig. 1(b). The drag coefficient was observed for various wind speeds ranging from 2 to $150\,\text{m/s}$. It can be observed that due to the smooth air flow through the shark-fin cover, the drag coefficient is lesser and stable than that of the rectangular shaped cover. The shark-fin cover with
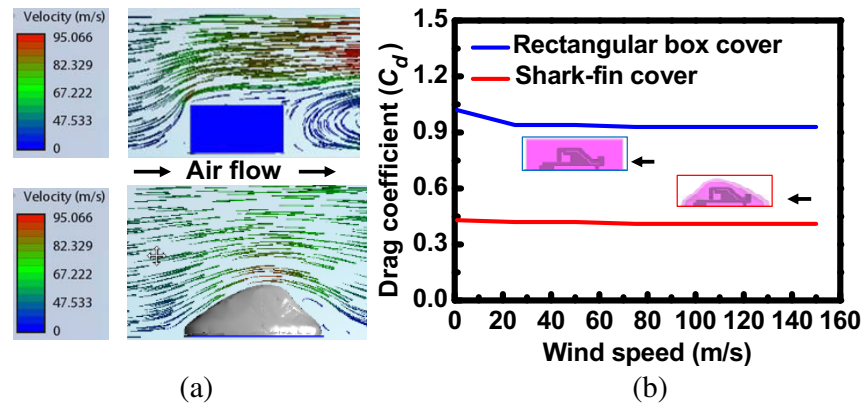
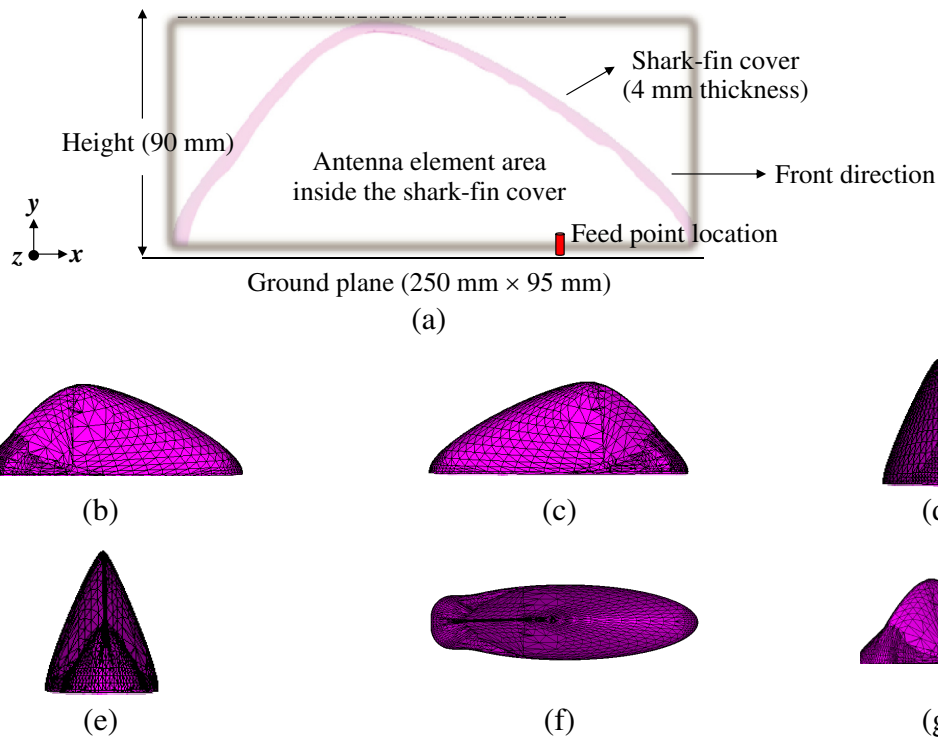**Figure 1.** Cover studies. (a) Air flow scenario. (b) Drag coefficient observation.

Figure 2. Shark-fin cover structure (various views). (a) Shark-fin cover outer layer. (b) Front towards-right view. (c) Front toward-left side view. (d) Front view. (e) Back-side view. (f) Top view. (g) Perspective view.

dimensions, such as height and thickness, and the ground plane on which the cover is fixed is shown in Fig. 2(a). In this figure, the antenna element area inside the shark-fin cover and the feed point location is also shown for the initial. The various views of the shark-fin cover are shown in Figs. 2(b)–(g) for better representation in 3D-scenario.

3. ANTENNA DESIGN PROCEDURE

The proposed antenna element geometry is shown in Fig. 3. The distance between the shorting pin/area and the antenna feed point is 106 mm as the IFA configuration was used. h is the parameter which shows the height of the element from the ground level. $a \times b$ represents an area near the feed point
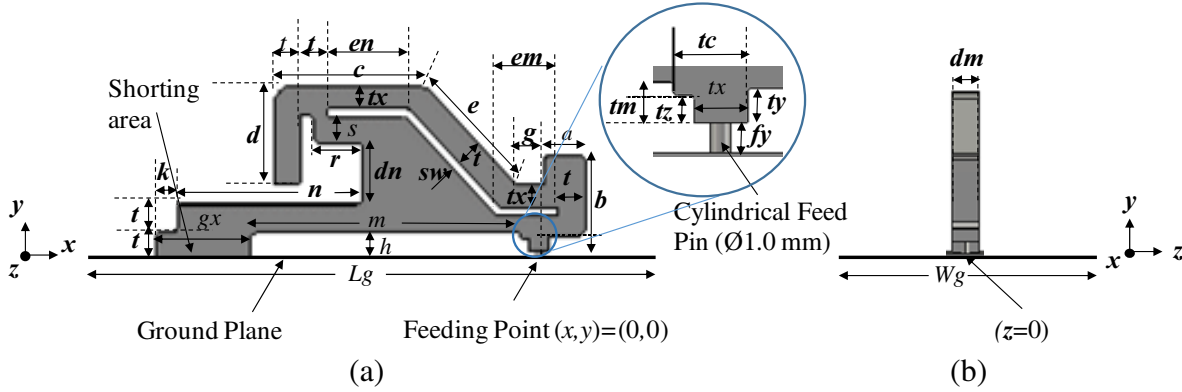
Figure 3. Proposed antenna design geometry, (a) x-y plane view, (b) y-z plane view.

(front side) used for impedance match at higher frequencies. d is the open stub length/dimension from the top point of the element as seen in the figure.

The design process is initiated with a theoretical calculation to estimate the antenna geometrical dimensions. In our case, the design is based on an inverted F-antenna configuration, where a thick square cross-sectional rod metal structure is used to design the antenna element. The inverted-F antenna can be understood as a variant of the monopole where the top section has been folded down so as to be parallel with the antenna ground plane. This is done to reduce the height of the antenna, while maintaining a resonant trace length. The parallel section of this type of antenna introduces capacitance to the input impedance of the antenna, which is compensated by implementing a short-circuit stub or short-circuiting plate. The stub's end is connected to the ground plane through a via in general.

The S-parameters of the initial element (Segment 1 in inset along with the cover layer) along with the current path for the lower band of interest (i.e., 700-MHz band) is shown in Fig. 4(a). The initial element is chosen to be thick (dm of 10 mm) to provide the mechanical strength for the antenna element to be fixed well on the antenna ground plane for railway application. The maximum usable size of the element was obtained theoretically in regard to the lowest frequency of operation [25]. The length of current path#1, which equals the sum of m, h, and a, matches the quarter wavelength at 700 MHz frequency, and brings about a resonance at 700 MHz in Fig. 4(a). However, the poor impedance matching results in high reflection, which should be modified by adding a part in Segment 2. On the other hand, the higher bands can be observed resonant at 3.2 GHz and 4.18 GHz with S_{11} below -10 dB level. This is contributed from the loop configuration formed by the feeding pin, main element shorting area, and the ground plane. Based on this initial element, three Segments are incorporated to create a greater number of resonances over the frequency band of interests and better impedance matching. The Segment 2 of Fig. 4(b) and the Segment 3 of Fig. 4(c) represent the generation of lower band (i.e., 700 MHz band) with required wideband characteristics, and the Segment 4 in Fig. 4(d) represents the generation of higher band (2100/3500 MHz band) along with the impedance matching for the complete antenna design process.

3.1. Lower Band (700 MHz Band)

In general, the Inverted-F antenna bandwidth is narrow, while the bandwidth requirement for 700 MHz band is wider ($\sim$ 70 MHz) in this application. Therefore, along with the impedance matching, other resonant current paths are created in a way that they resonate with the nearby frequencies (length $= \pm\lambda/4$) and also have the conformal size to be fitted in the cover. This configuration results in the wideband behavior at the 700 MHz band. Segment 2 is designed from the initial inverted antenna configuration by adding a part corresponding to the length ($dn + r + d$) to the center point of the F-shaped element. By adding this part, the configuration provides the current path#2 (Fig. 4(b)) with a total length of ($h + dn + d + r + t$). Those multiple paths create a strong resonance at 710 MHz with the minimum S_{11} of -12 dB in Fig. 4(b). It is also noticeable that the frequency response at the high frequencies has changed from that of Segment 1, because the loop configuration is modified while
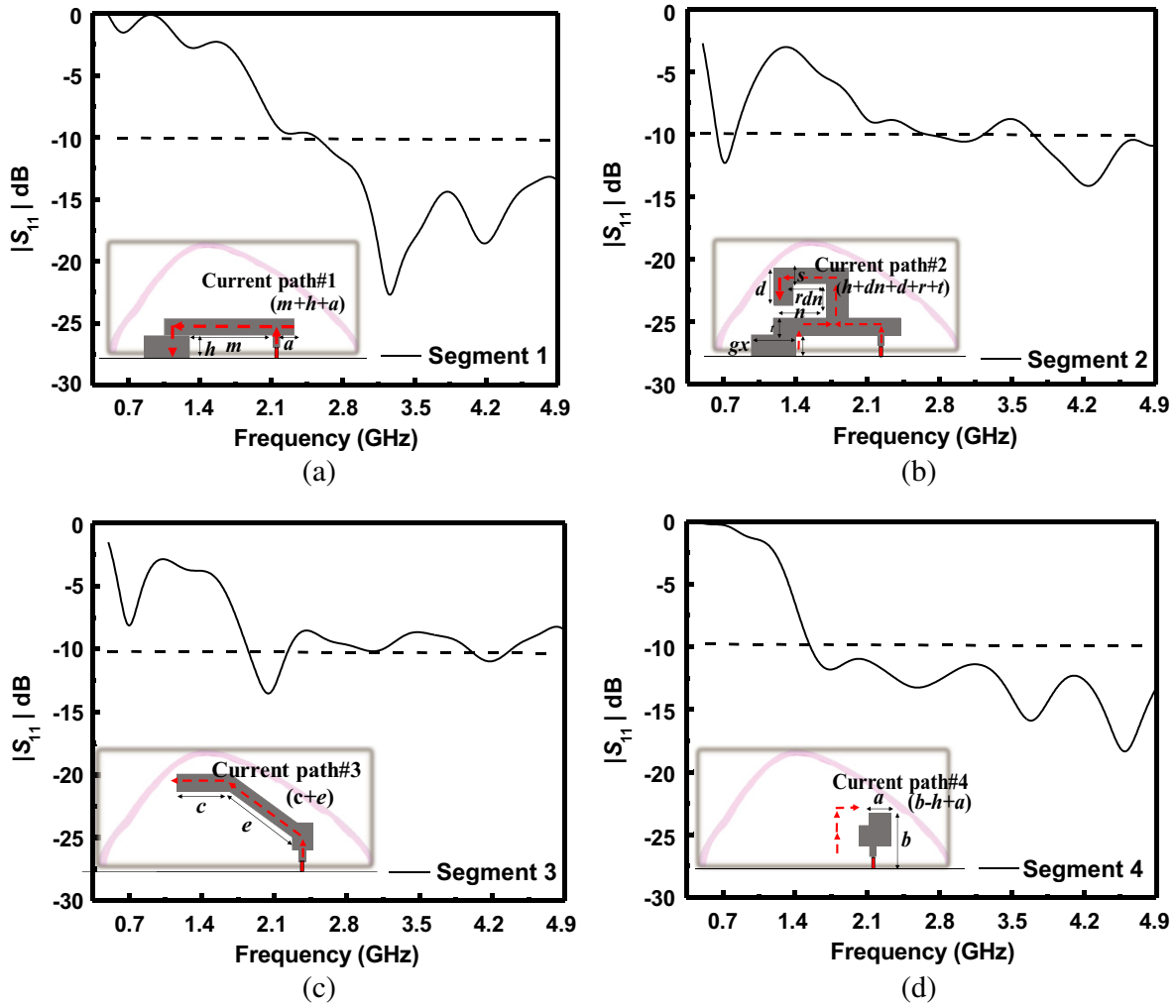
Figure 4. Antenna element design segments: initial S-parameters. (a) Segment 1. (b) Segment 2. (c) Segment 3. (d) Segment 4.

incorporating the additional part in Segment 2.

To widen the bandwidth at 700 MHz as required, additional current path#3 (Segment 3) was created as shown in Fig. 4(c). Since the length of this current path $(c + e)$ is only a few millimeters longer than the quarter wavelength, this configuration gives the resonance at 690 MHz with -8 dB minimum S_{11} value, as a bent monopole above the ground plane. Moreover, it creates multiple higher order modes in addition to the fundamental resonance at 690 MHz, which is beneficial for wideband operation.

3.2. Higher Band (2100/3500 MHz Band)

The railway communication requires to include the LTE and Lower 5G band, i.e., 2100 MHz and 3500 MHz frequency bands, in a single feed shark-fin antenna structure. To fulfill the requirement, Segment 4 (inset of the Fig. 4(d)) is accommodated in the antenna design, and the S-parameters are shown in Fig. 4(d). The current path#4 with a length of $(b - h + a)$ plays an important role in these bands. This element has no effect on the 700 MHz band and has the resonances in the higher band only. A wideband behavior is observed as well with $S_{11} < -10$ dB in a single quarter wavelength monopole case. Such a wide bandwidth of the monopole can be explained by the thick ($dm = 10$ mm) metal rod resulting in the low quality factor. This length of monopole (Segment 4) with the combination of the

harmonics of the lower band element (Segment 2 and Segment 3) is responsible for the operation in the high frequency band.

All the Segments are combined to form a complete structure (Fig. 3), which can be fitted well inside the shark-fin cover and thus having the required operating frequency bands for the railway communications. As a last step to finalize the antenna geometry, the parametric analysis is done as described in the next section.

3.3. Parametric Analysis of the Complete Antenna

The antenna design parameters such as a, b, d, h, and metal thickness (dm) have significant effect on the antenna performance. In the parametric study, the high-end points of parameters are set in a way that the antenna element should not intersect with the shark-fin cover or any other parts of the antenna element beyond. Figs. 5(a)–(f) show the parametric study of the proposed antenna element to analyze the antenna performance. For each plot, each parameter is varied in a range while the other key parameters are kept fixed at the high-end values. The parameters are selected in a way to yield the widest operation range of the antenna.
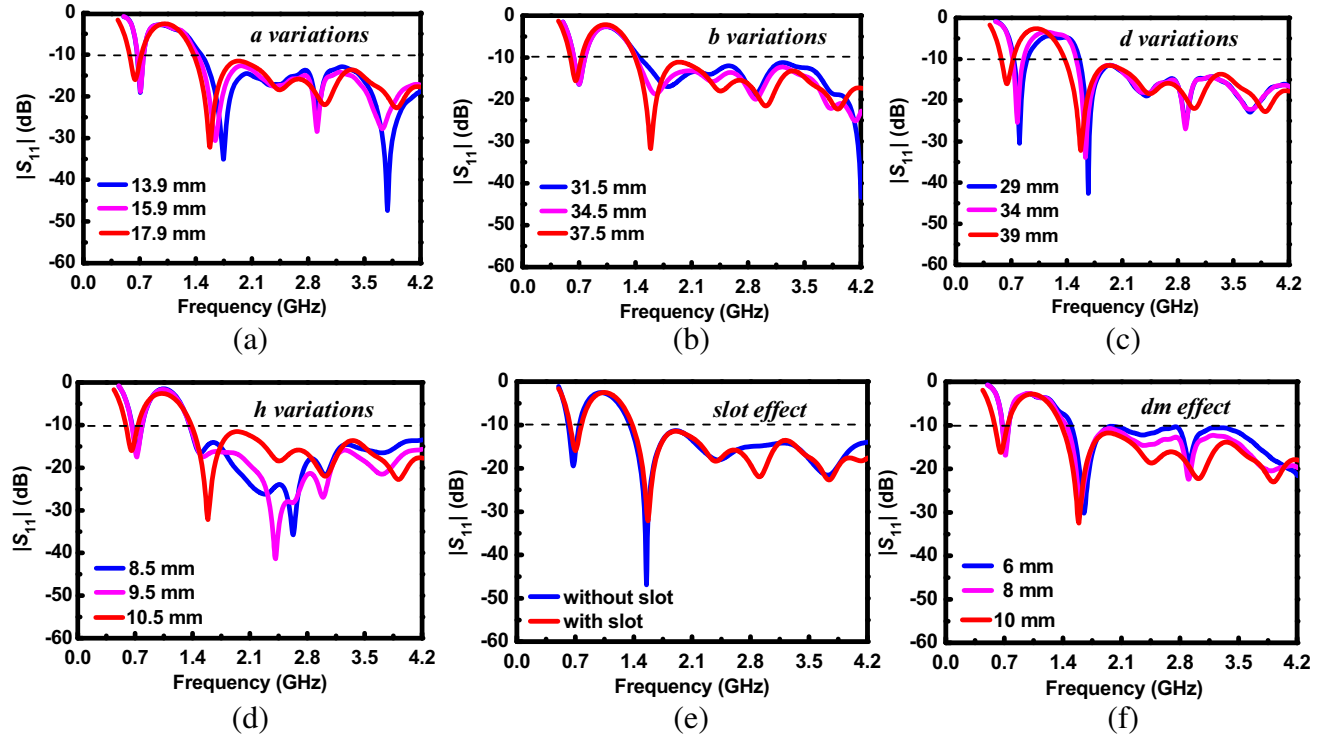

Figure 5. Antenna geometry parametric study: the shark-fin antenna.

For example, from Figs. 5(a) and (b), when a and b are at high-end values, the wideband performance is achieved at the lower frequency band, and a small shift can be observed at the higher band. From Fig. 5(c), parameter d plays a key role in the parametric analysis. When d increases, the lower frequency band shifts toward the lower end, and the higher frequency band is also extended. This parameter in Segment 2 efficiently tunes the frequency at the lower band along with the starting frequency point of the higher band. The parameter h is determined to make the lower frequency bandwidth widest (Fig. 5(d)), and the effect of slot width is also studied (Fig. 5(e)). Most of all, the metal thickness of the antenna element (dm) is an important parameter on the frequency response of the antennas. From Fig. 5(f), the increase of thickness achieves better impedance match over a wide range of frequencies including 700 MHz, 2100 MHz, and 3500 MHz bands by lowering the quality factor.
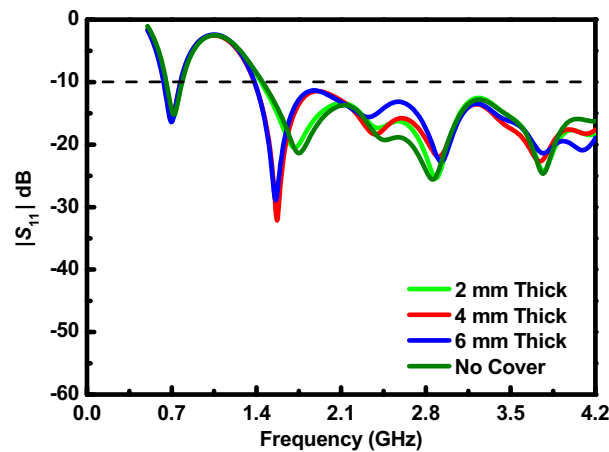
Figure 6. Antenna element with various covers.

3.4. Effect of the Shark-Fin Cover Thickness

Since the presence and thickness of shark-fin cover affect the near field of an antenna, its effect is simulated as shown in Fig. 6. As the thickness of the cover increases from 2 mm to 6 mm, the antenna performance remains relatively the same as long as the gap between the antenna and the cover is more than 5 mm. Since the cover thickness does not affect the electrical performance in bandwidth, the thickness is determined based on mechanical preference. In this work, the thickness of 4 mm is used to cover the antenna since it provides the strength to itself as compared to the thin cover of 2 mm. The cover can be fixed by the nuts and bolts on the ground plane of antenna.
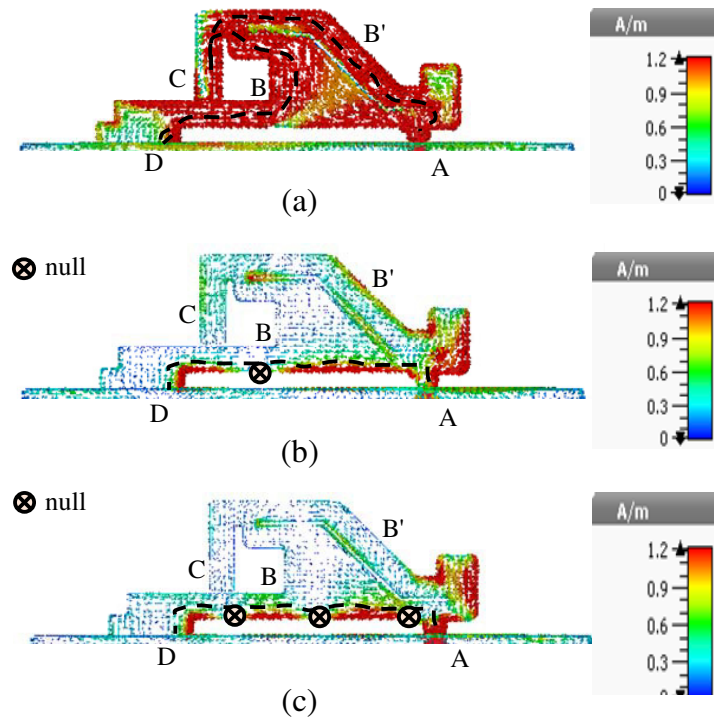

Figure 7. Current distribution. (a) 700 MHz, (b) 2100 MHz, (c) 3500 MHz.

3.5. Current Distribution

The multiband operation of antenna can also be explained from its current distribution at selected frequencies in the complete antenna geometry. The current distribution for the required frequencies is shown in Figs. 7(a)–(c). For 700-MHz band, the two current paths can be seen as AB'C and DBC which respond to the approximate length as of $\lambda/4$ and that can be observed as an inverted-F antenna configuration (Segment 1, Segment 2, and Segment 3), where A is the feeding point, and D is the ground connection point to the antenna. For 2100 MHz, the current distribution can be observed with a single null, and the current path has a length of approximately 106 mm (loop length ABD) which represents 0.75λ mode of operation as seen in Fig. 7(b). Similarly, the current path ABD (loop length) in Fig. 7(c) represents 3 nulls and a length of approximately $3/2\lambda$ for 3500 MHz frequency band. The current at higher band frequencies is mostly confined in the loop configuration in Segment 2 and Segment 4. These multiple resonances cause the multiband operation of antenna at the desired frequencies.
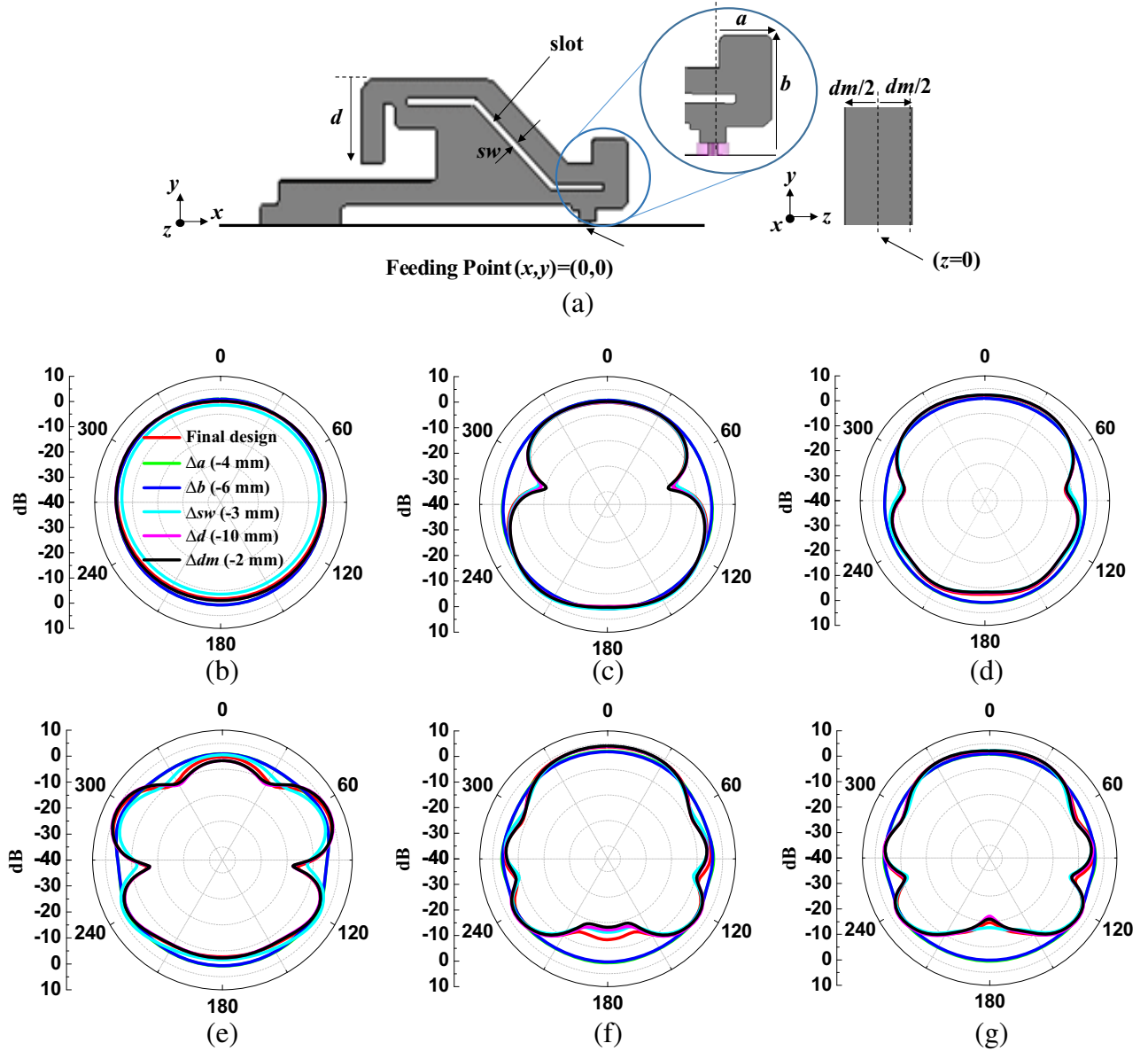

Figure 8. Effect of various parameters in the radiation performance. (a) Proposed antenna geometry with critical parameters, (b) 700 MHz, 1600 MHz, (d) 2100 MHz, (e) 2800 MHz, (f) 3500 MHz, (g) 3800 MHz.

3.6. Effect on the Radiation Performance of Various Parameters

Further, the effect of these parameters on the radiation pattern is also studied for the frequency points at which $S_{11} < -10$ dB. As in Fig. 5, the effect of the selected parameters a, b, d, sw, and the metal thickness (dm) is studied in terms of the radiation patterns (Fig. 8(a)). The effect of those parameters (in terms of Δ, the difference from the final design parameter) on the radiation performance is shown in Fig. 8. Here the horizontal plane patterns are shown for the various frequency points with $S_{11} < -10$ dB.

Parameters a and b are the key parameters to observe the effect on the radiation performance compared to the final design. It can be observed that if a and b decrease, the radiation patterns become more omnidirectional, especially for the 2100 MHz/2800 MHz/3500 MHz/3800 MHz bands. Nevertheless, a and b are chosen to be 17.9 mm and 37.5 mm to ensure the broadest frequency operation. Other parameters such as sw, d, and dm have minimal effects on the radiation patterns in Fig. 8. As a result, the proposed shark-fin antenna is optimized with all the parameters discussed above by using the parametric analysis, and final parameters values are summarized in Table 1.

Table 1. Final antenna design parameters (all dimensions are in mm).

gx	36.0	a	17.9	em	22.8	d	39.0	tm	6.0	ty	5.0
h	10.5	b	37.5	m	103.0	n	70.7	tx	8.0	k	8.2
t	10.5	g	10.5	en	36.9	r	19.0	tz	4.0	fy	4.5
dn	21.4	e	48.3	c	55.6	s	9.1	tc	11.0	sw	3.0

To summarize the simulation results, the antenna operates at multiband frequencies in a range of 0.5–4.2 GHz. The stopband is also observed in between the lower band and higher band because of the no existence of any higher order mode for the 700 MHz band. Nevertheless, the proposed antenna can work on multiple frequency bands, including the frequency bands of 700 MHz, 2100 MHz, and 3500 MHz, which are the main interests of this research. In the next section, S_{11} parameter and radiation patterns in horizontal xz-plane for these frequency bands are measured and validated for the advanced railway communications.

4. MEASUREMENT RESULTS AND DISCUSSION

The proposed shark-fin antenna (antenna element, ground plane and cover) is fabricated with the 3D printing technique using the white color ABS material, and then the copper tape was wrapped around on the surfaces of antenna element and ground plane to make the antenna structure conductive.

The feeding pin (1-mm diameter) was soldered to the antenna element. The fabricated antenna element including the shark-fin cover can be seen in Fig. 9. The S-parameters of the proposed designed
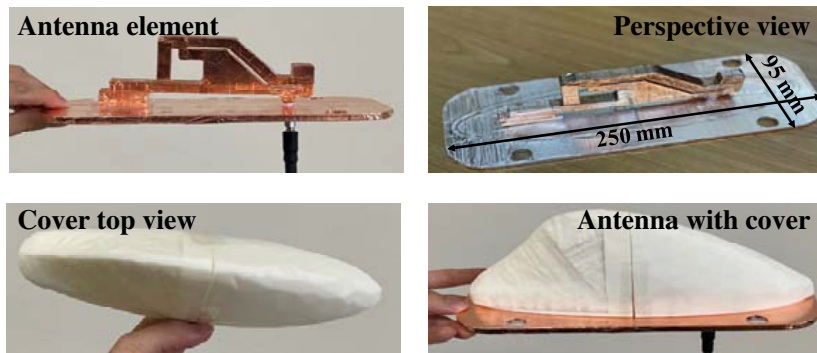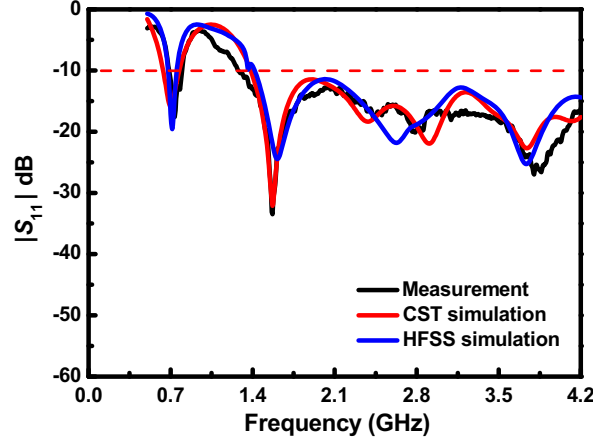

Figure 9. The fabricated antenna structure.

Figure 10. Simulated and measured S-parameters.

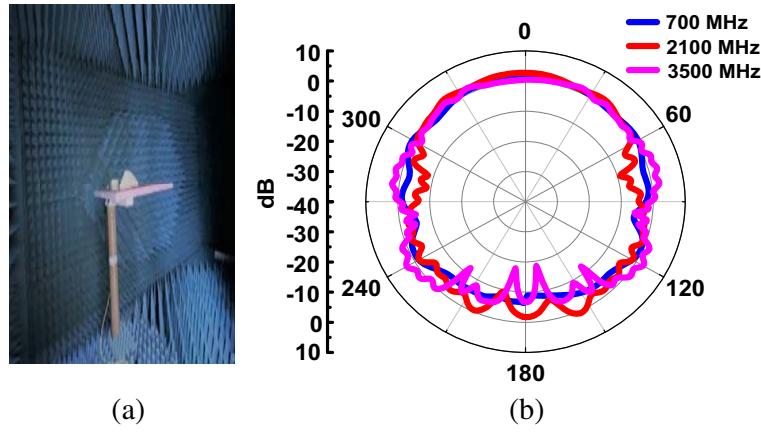(a)   (b)

Figure 11. (a) Antenna in anechoic chamber, (b) measured antenna radiation pattern (horizontal-xz plane).

antenna are shown in Fig. 10. The simulation results from both CST and HFSS match well with the measurement ones for the required bands. It is observed that the proposed antenna is resonant at LTE-R, LTE, and lower 5G bands with $S_{11} \leq -10$ dB. The impedance bandwidth is observed as 110 MHz (690–800 MHz) for 700-MHz band. It can also be seen that a wide band behavior is observed from 1.4–4.2 GHz band resulting in the significant antenna bandwidth required for LTE (2100 MHz) and lower 5G (3500 MHz) bands for railways communications. The radiation pattern of the antenna is measured in an anechoic chamber as shown in Fig. 11(a) for the required frequencies and plotted in Fig. 11(b) for the horizontal xz-plane. As preferred for vehicular antennas [21], the pattern is almost omnidirectional in the horizontal plane for the required frequencies. Although it is not shown in the figure, the maximum antenna gain was measured to be 2.28 dBi for 700 MHz, 4.6 dBi for 2100 MHz, and 6.4 dBi for 3500 MHz. The antenna efficiency for each frequency is 64.8%, 95.8%, and 98.8%.

To ensure that a large metal surface of train rooftop does not ruin the multiband operation of the antenna when it is deployed, the proposed shark-fin antenna is also tested on the train roof for the performance evaluation. For the measurement setup, the ground plane of the shark-fin antenna is extended up to 610 mm × 455 mm (the ground size of antenna was 250 mm × 95 mm in Fig. 10) by using the copper sheet and fixed well with the copper tape. A gap of 7.5 cm is also kept in between the roof and ground plane for making the coaxial cable connections from the VNA. The measurement was performed on a train standing at Korean Railroad Research Institute as shown in Fig. 12(a). It can be observed in Fig. 12(b) that the antenna performance is stable in the required higher operating bands. A slight shift in the response on the roof can be due to the longer current paths due to the larger ground plane. The
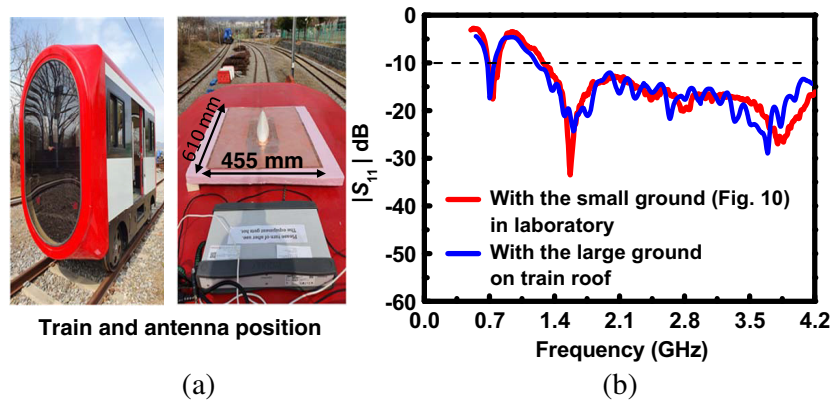
Figure 12. Measurement on train, (a) antenna on the train roof, (b) S-parameters.

proposed antenna with a large ground plane (in the train environment) has the efficiencies of 71.7%, 92.6%, and 96.4 % for the LTE-R, LTE, and Lower 5G band frequencies, respectively. The proposed shark-fin antenna satisfies the required multiband specification for the advanced railway communications and is ready for the deployment.

5. CONCLUSION

In this paper, a shark-fin antenna is studied in detail for the future advance railways. The airflow simulation confirms the lower air resistivity of the proposed shark-fin cover than the rectangular cover. As a result of parameter optimization, more than 70-MHz bandwidth is obtained for the 700-MHz applications in the real scenario of examination on the train roof. Further, the sufficient bandwidths for the other required bands (2100 MHz and 3500 MHz) are obtained as wide band frequency behavior starts from 1.4 GHz to 4.2 GHz. The proposed antenna has omnidirectional radiation patterns as preferred for vehicular antenna in horizontal plane for all the required frequencies. The antenna gain is observed as 2.28 dBi, 4.6 dBi, and 6.4 dBi for the frequencies 700 MHz, 2100 MHz, and 3.5 GHz, respectively. The antenna has the efficiencies of 64.8%, 95.8%, and 98.8% for the LTE-R, LTE, and lower 5G bands, respectively. In the actual train environment (large ground scenario), the antenna has the efficiencies of 71.7%, 92.6%, and 96.4% for the LTE-R, LTE, and lower 5G bands, respectively. The integration of RF modules with the proposed antenna and characterization will be the future scope for this work.

REFERENCES

1. Choi, J. K., H. Cho, H. S. Oh, K. H. Kim, M. J. Bhang, I. S. Yu, and H. G. Ryu, "Challenges of LTE high-speed railway network to coexist with LTE public safety network," *International Conference on Advanced Communication Technology, ICACT*, 524–528, 2015.

2. Cheng, Y., J. Lu, and C. Wang, "Design of a multiple band vehicle-mounted antenna," *International Journal of Antennas and Propagation*, 1–11, 2019.

3. Arya, A. K., S. J. Kim, and S. Kim, "A dual-band antenna for LTE-R and 5G lower frequency operations," *Progress In Electromagnetics Research Letters*, Vol. 88, 113–119, 2020.

4. Choi, H. Y., Y. Song, and Y. K. Kim, "Standards of future railway wireless communication in Korea," *Recent Advances in Computer Engineering, Communications and Information Technology*, 360–367, 2014.

5. Wang, H. and G. Yang, "Design of 4×4 microstrip quasi-yagi beam-steering antenna array operation at 3.5 GHz for future 5G vehicle applications," *International Workshop on Antenna Technology: Small Antennas, Innovative Structures, and Applications (iWAT)*, 2017.

6. Fujita, K., "MNL-FDTD/SPICE method for fast analysis of short-gap ESD in complex systems," *IEEE Transactions on Electromagnetic Compatibility*, Vol. 58, No. 3, 709–720, June 2016.

7. Wang, S., K. M. Mak, H. W. Lai, K. K. So, Q. Xue, and G. Liao, "Printed circularly polarized wire antennas with DC grounded stub," *Microwave and Optical Technology Letters*, 2719–2725, December 2012.

8. Basaery, D., S. Hosein, M. Armaki, and S. M. J. Razavi, "Radiation pattern analysis of inverted-F antenna mounted on the side wall of a long cylinder," *Journal of Communication Engineering*, Vol. 7, No. 2, 2018.

9. Huang, K., W. T. Hung, T. H. Cheng, and S. Y. Chen, "A 2.45-GHz high-efficiency loop-shaped PIFA rectenna for portable devices and wireless sensors," *IEEE International Symposium on Antennas and Propagation & USNC/URSI National Radio Science Meeting*, 1284–1285, 2015.

10. Henningsson, P. and A. Hedenström, "Aerodynamics of gliding flight in common swifts," *Journal of Experimental Biology*, 382–393, 2010.

11. Shavit, R., *Radome Electromagnetic Theory and Design*, Willey-IEEE Press, 2018.

12. Wu, Q., Y. Zhou, and S. Guo, "An L-sleeve L-monopole antenna fitting a shark-fin module for vehicular LTE, WLAN, and car-to-car communications," *IEEE Transactions on Vehicular Technology*, Vol. 67, No. 8, 7170–7180, 2018.

13. Ghafari, E., A. Fuchs, D. Eblenkamp, and D. N. Aloi, "A vehicular rooftop, shark-fin, multiband antenna for the GPS/LTE/cellular/DSRC systems," *IEEE-APS Topical Conference on Antennas and Propagation in Wireless Communications (APWC)*, 237–240, 2014.

14. Liu, Y., Z. Ai, G. Liu, and Y. Jia, "An integrated shark-fin antenna for MIMO-LTE, FM, and GPS applications," *IEEE Antennas and Wireless Propagation Letters*, Vol. 18, No. 8, 1666–1670, 2019.

15. Kwon, O. Y., R. Song, and B. S. Kim, "A fully integrated shark-fin antenna for MIMO-LTE, GPS, WLAN, and WAVE applications," *IEEE Antennas and Wireless Propagation Letters*, Vol. 17, No. 4, 600–603, 2018.

16. Melli, F., S. Lenzini, M. Cerretelli, E. Coscelli, A. Notari, S. Selleri, and L. Vincetti, "Low profile wideband 3D antenna for roof-top LTE vehicular applications," *IEEE-APS Topical Conference on Antennas and Propagation in Wireless Communications (APWC)*, 2019.

17. Software, Autodesk flow design, available online: https://www.autodesk.com/education/free-software/flow-design.

18. Software, CST studio suite, http://sst-mea.com/home.html.

19. Software, Ansys HFSS, https://www.ansys.com/products/-electronics/ansys-hfss.

20. Ribeiro, A. G., "Analysis of antennas' locations on trains for mobile communications," Thesis, Universidade de Lisboa, 2018.

21. Williams, D. J. S., "Train roof antenna positioning issue study," *Rail Safety and Standards Board (RSSB) Research Project T739*, Siemens Mobility, London, UK, July 2009.

22. Lu, Y., K. Xiong, P. Fan, Y. Zhang, and Z. Zhong, "Deploying multiple antennas on high-speed trains: Equidistant strategy vs fixed-interval strategy," *Proc. of 2016 IEEE 84th Vehicular Technology Conference (VTC-Fall)*, Montreal, Canada, September 2016.

23. Pals, V. A. F., "Analysis of influence on antenna radiation patterns by conducting environments for the development of vehicle antennas," Thesis, Technische Universität München, München, Germany, 2013.

24. Elfergani, I., A. S. Hussaini, J. Rodriguez, and R. A. Alhameed, *Antenna Fundamentals for Legacy Mobile Applications and Beyond*, Springer International Publishing, 2018.

25. Wong, K. L., *Planar Antennas for Wireless Communications*, John Wiley & Sons, 2003.